Supplementary Information
Cyclodextrin and Modified Cyclodextrin Complexes of *E*-4-*t*-butylphenyl-4'-oxyazobenzene: UV-Visible, ^{1}H NMR and *Ab Initio* Studies

Bruce L. May,[a] Jacobus Gerber,[a] Philip Clements,[a] Mark A. Buntine,[a] David R. B. Brittain,[a] Stephen F. Lincoln*[a] and Christopher J. Easton[b]

[a] *Department of Chemistry, University of Adelaide, Adelaide, SA 5005, Australia. E-mail:Stephen.Lincoln@adelaide.edu.au*
[b] *Research School of Chemistry, Australian National University, Canberra, ACT 0200, Australia.*

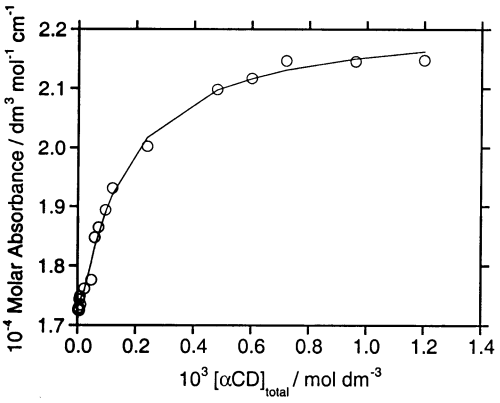

Fig. S1. The variation of the absorbance of *E*-**3**$^-$ at 400 nm with increase in $[\alpha CD]_{total}$. The solid curve represents the best fit of the algorithm for the formation of $\alpha CD \cdot \mathbf{3}^-$ and $(\alpha CD)_2 \cdot \mathbf{3}^-$ to the experimental data over the λ ranges 375-420 nm and 430-500 nm.

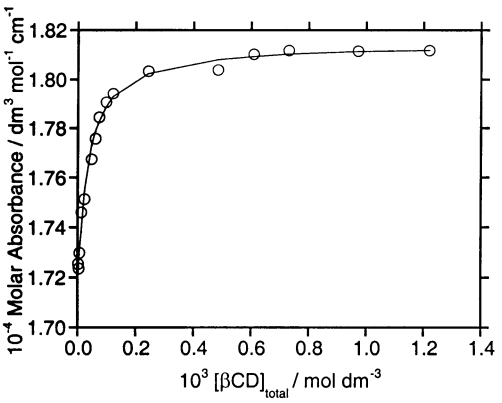

Fig. S2. The variation of the absorbance of *E*-**3**$^-$ at 400 nm with increase in $[\beta CD]_{total}$. The solid curve represents the best fit of the algorithm for the formation of $\beta CD \cdot \mathbf{3}^-$ and $(\beta CD)_2 \cdot \mathbf{3}^-$ to the experimental data over the λ ranges 387-413 nm and 425-445 nm.

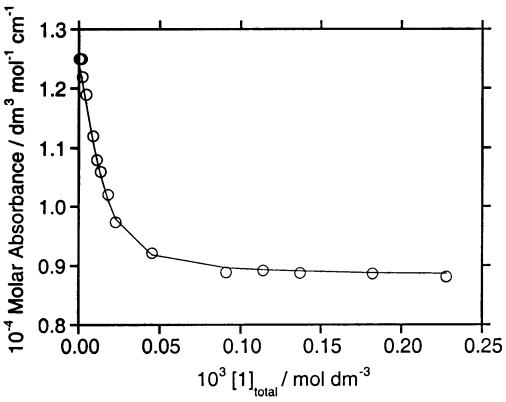

Fig. S3. The variation of the absorbance of *E*-**3**$^-$ at 370 nm with increase in $[\mathbf{1}]_{total}$. The solid curve represents the best fit of the algorithm for the formation of **1**·**3**$^-$ and to the experimental data over the λ range 300-500 nm.

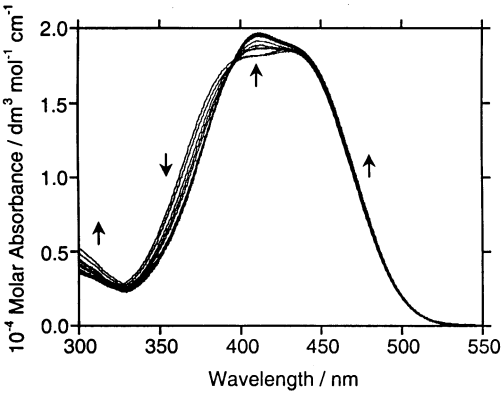

Fig. S4. The change in the UV-visible absorbance of *E*-**3**$^-$ (indicated by arrows) with increase in $[\mathbf{2}]_{total}$ in aqueous solution at pH 10.0, 298.2 K and I = 0.10 mol dm^{-3} (Et_4NClO_4). $[E\text{-}\mathbf{3}^-]_{total}$ = 1.92 x 10^{-5} mol dm^{-3} and $[\mathbf{2}]_{total}$ = 2.14 x 10^{-6}-2.14 x 10^{-4} mol dm^{-3}.

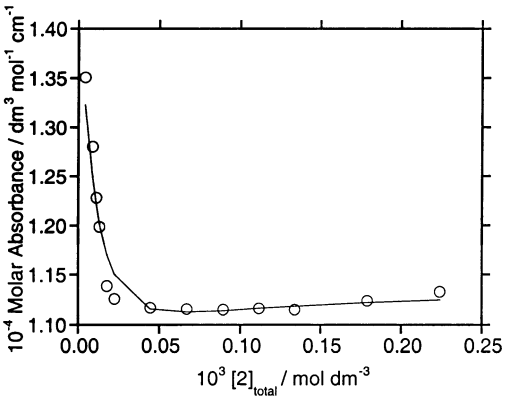

Fig. S5. The variation of the absorbance of *E*-**3**$^-$ at 370 nm with increase in $[\mathbf{2}]_{total}$. The solid curve represents the best fit of the algorithm for the formation of **2**·**3**$^-$ and $(\mathbf{2})_2$·**3**$^-$ to the experimental data over the λ range 350-430 nm.

Fig. S6. Representative variable temperature ^{1}H NMR (600 MHz) spectra of the aromatic protons of *E*-**3**$^-$ in αCD·*E*-**3**$^-$ showing their assignments. The spectra are not plotted to a constant vertical scale. The solution is 0.01 mol dm^{-3} in αCD and in *E*-**3**$^-$ in 0.10 mol dm^{-3} NaOD.

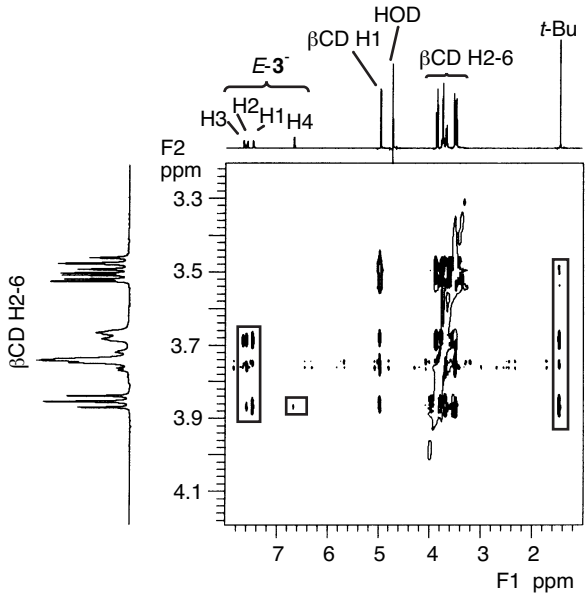

Fig. S7. ^{1}H 600 MHz ROESY NMR spectrum of 0.02 mol dm^{-3} βCD and 0.01 mol dm^{-3} E-**3**$^{-}$, which exist dominantly as (βCD)$_2$·E-**3**$^{-}$ in 0.10 mol dm^{-3} NaOD at 298 K. The cross-peaks enclosed in the rectangles correspond to NOE interactions between the protons indicated on the F1 and F2 axes.

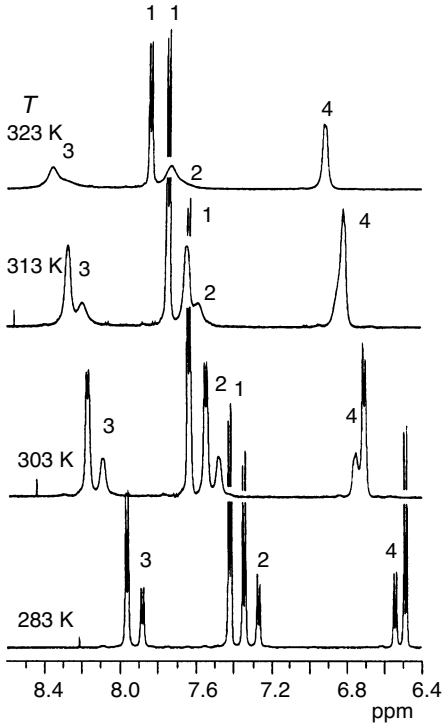

Fig. S8. Representative variable temperature ^{1}H NMR (600 MHz) spectra of the aromatic protons of *E*-**3**$^{-}$ in (αCD)$_2$·*E*-**3**$^{-}$ showing their assignments. The spectra are not plotted to a constant vertical scale. The solution is 0.06 mol dm^{-3} in αCD and 0.02 mol dm^{-3} in E-**3**$^{-}$ in 0.10 mol dm^{-3} NaOD.

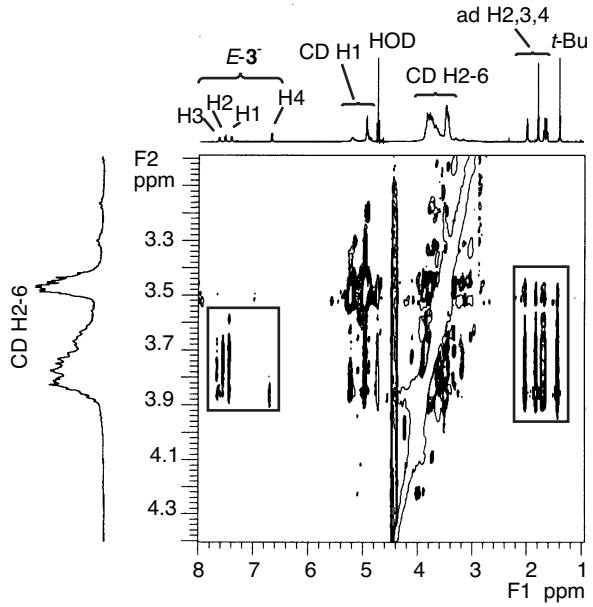

Fig. S9. ^{1}H 600 MHz ROESY NMR spectrum of 0.01 mol dm^{-3} **2**, E-**3**$^{-}$ and **6**$^{-}$ (ad) which exist dominantly as **2**·E-**3**$^{-}$·**6**$^{-}$ in 0.10 mol dm^{-3} NaOD at 298 K. The cross-peaks enclosed in the rectangles correspond to NOE interactions between the protons indicated on the F1 and F2 axes.

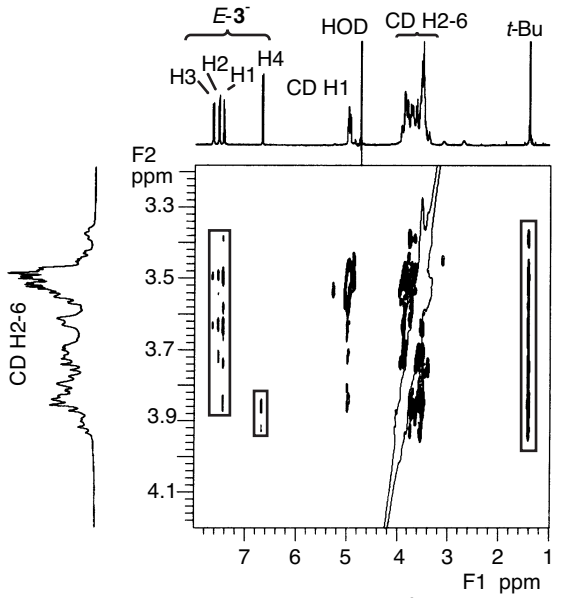

Fig. S10. ^{1}H 600 ROESY NMR spectrum of 0.01 mol dm^{-3} **2** and 0.02 mol dm^{-3} in *E*-**3**$^{-}$, which exists dominantly as **2**·(*E*-**3**$^{-}$)$_2$ in 0.10 mol dm^{-3} NaOD at 298 K. The cross-peaks enclosed in the rectangles correspond to NOE interactions between the protons indicated on the F1 and F2 axes.

Ab Initio Results and Methods

Table 3 contains a list of selected interatomic parameters, as well as the absolute and relative energies for stationary points on the ground electronic potential energy surface of 4-*t*-butyl-phenyl-4-hydroxyazobenzene (*E*-**3**H and *Z*-**3**H). Fig. S11 shows the optimised geometries of each stationary point. The energetic data at the HF/6-31g(d,p) level of theory are generally unremarkable and indicate that the ground-state barrier to conversion from *E*-**3**H to *Z*-**3**H is 203.7 kJ mol^{-1}, whereas the reverse barrier for isomerization from *Z*-**3**H and *E*-**3**H is 128.6 kJ mol^{-1}. Thus, possibility i) that a relatively small barrier exists for isomerization from *Z*-**3**H and *E*-**3**H, can be discounted and *E*-**3**H is seen to be the thermodynamically favoured isomer. Calculations performed at the B3LYP/6-31g(d,p) level of theory predict corresponding barriers of 169.1 and 105.8 kJ mol^{-1} and indicate that the presence of a substantial of a reverse barrier is independent of the level of theory employed. Under the experimental conditions *E*-**3**H is deprotonated to form *E*-**3**$^-$ and HF/6-31g(d,p) calculations show that the barrier to isomerization from *E*-**3**$^-$ to *Z*-**3**$^-$ is 183.1 kJ mol^{-1} and that for isomerization from *Z*-**3**$^-$ and *E*-**3**$^-$ is 105.9 kJ mol^{-1} consistent with deprotonation having little overall effect.

Considerable effort has been expended recently in attempts to elucidate the mechanistic aspects of *E*-*Z* isomerization in azobenzene.[S1-S4] This process has been postulated to proceed through either a "rotation" mechanism involving a twisting around the N-N bond, or an "inversion" mechanism occurring about one of the C-N-N angles.[S2] Inspection of the ground state reaction coordinate for **3**H indicates that an inversion mechanism operates. This is evidenced by the significant difference in the C-N bond lengths in the transition state structure, as well as the near linearity of N-N-C angle for the 4'-hydroxybenzene carbon. Consistent with our results, Cattaneo and Persico[S1] showed that the thermal isomerization of azobenzene involves an inversion mechanism.

Insight into the photoisomerization process requires an investigation of the excited electronic states of **3**H. In this study the configuration interaction involving single electron excitations (CI-Singles) approach has been employed. Previous theoretical studies of the photoisomerization processes in azobenzene[S5] have indicated that the S_1 state has a transoid minimum energy conformation with a CNNC dihedral angle nearing 180^o, while the S_2 state has a twisted minimum involving a deep energy well at a CNNC dihedral angle of ~100^o. These earlier studies show that the S_1 state involves the n-π^* transitions in azobenzene, whilst the π- π^* transitions involves both the S_1 and S_2 states. In contrast, the minium energy conformation of the **3**H S_1

excited electronic state found in this study has a CNNC dihedral of 113.2°. (Selected geometric parameters as well as energetic data describing this conformation appear in Table 3.) It is clear that the photochemistry of **3**H differs, in part, from that of azobenzene due to the markedly different shape of the S_1 excited electronic state. Although retaining a transoid configuration, as is the case for azobenzene, **3**H adopts a twisted S_1 minimum energy conformation with a CNNC dihedral angle of 113.2° (lower view in Fig. S12). This suggests that if the **3**H photoisomerization process involves the S_1 excited electronic state predominantly, there may be little opportunity, short of introducing significant vibrational or other internal excitation into the S_1 state, to access cisoid configurations. This interpretation is consistent with no *E*-**3**$^-$ to *Z*-**3**$^-$ isomerization being observed in this study.

As mentioned above, the π-π^* transitions in azobenzene involve both the S_1 and S_2 excited electronic states.[S1] Thus, it is appropriate to identify the key stationary points on the S_2 surface of **3**H. Attempts to identify the minimum energy conformation using the CI-Singles approach proved unsuccessful. The most likely reason for this is that the S_2 state mixes with another electronic state with a geometry incorporating a CNNC dihedral angle of ~155°. The CI-Singles approach is not a suitable choice of computational method under these circumstances. Nevertheless, a series of single-point energy calculations where all internal stereochemical parameters were fixed at the S_1 minimum geometry values and only the CNNC dihedral angle were varied indicated that the S_2 minimum energy configuration of **3**H is strongly transoid. Again, this result differs from the predictions of Cattaneo and Persico[S1] for azobenzene, but is consistent with no *E*-**3**$^-$ to *Z*-**3**$^-$ isomerization being observed in this study.

Ab initio calculations

All *ab initio* calculations were performed using the Gaussian 98 suite of programs using the Pople-type 6-31g(d,p) basis set.[S6] Ground electronic state calculations were performed at the Hartree-Fock level of theory, whilst calculations involving the S_1 and S_2 excited electronic states were performed using single-excitation configuration interaction (CI-Singles). Stationary points on each electronic potential energy surface were characterised as being minima or transition states by diagonalising the second-derivative Hessian matrix to determine the number of negative eigenvalues (0 for minima, 1 for transition states). The reported zero-point energies are unscaled. In order to verify that the transition states identified connected to the expected minima, intrinsic reaction coordinate (IRC) calculations were performed, in which the paths of steepest descent (in

mass-weighted Cartesian co-ordinates) were followed from the transition state of interest to the connecting minima. The default step size along the reaction path was 0.1 $amu^{1/2}$bohr.

References

S1. P. Cattaneo and M. Perisco, *Phys. Chem. Chem. Phys*, 1999, **1**, 4739.

S2. T. Ishikawa, T. Noro and T. Shoda, *J. Chem. Phys.*, 2001, **115**, 7503.

S3. Y. Hirose, H. Hiroharu and T. Sawada, *J. Phys. Chem. A*, 2002, **106**, 3067.

S4. T. Fujino, S. Y. Arzhantzev and Y. Tahara, *Bull. Chem. Soc. Jpn.*, 2002, **75**, 1031

S5. C. Gonzalez and H. B. Schlegel, *J. Chem. Phys*., 1989, **90**, 2154.

S6. Gaussian 98, Revision A.11.3, M. J. Frisch, G. W. Trucks, H. B. Schlegel, G. E. Scuseria, M. A. Robb, J. R. Cheeseman, V. G. Zakrzewski, J. A. Montgomery, R. E. Stratmann, J. C. Burant, S. Dapprich, J. M. Millam, A. D. Daniels, K. N. Kudin, M. C. Strain, O. Farkas, J. Tomasi, V. Barone, M. Cossi, R. Cammi, B. Mennucci, C. Pomelli, C. Adamo, S. Clifford, J. Ochterski, G. A. Petersson, P. Y. Ayala, Q. Cui, K. Morokuma, N. Rega, P. Salvador, J. J. Dannenberg, D. K. Malick, A. D. Rabuck, K. Raghavachari, J. B. Foresman, J. Cioslowski, J. V. Ortiz, A. G. Baboul, B. B. Stefanov, G. Liu, A. Liashenko, P. Piskorz, I. Komaromi, R. Gomperts, R. L. Martin, D. J. Fox, T. Keith, M. A. Al-Laham, C. Y. Peng, A. Nanayakkara, M. Challacombe, P. M. W. Gill, B. Johnson, W. Chen, M. W. Wong, J. L. Andres, C. Gonzalez, M. Head-Gordon, E. S. Replogle, and J. A. Pople, Gaussian, Inc., Pittsburgh PA, 2002.

Table 3. Selected bond distances, r_{NN} and r_{CN}, energies, zero-point energies (ZPE) and relative energies (E_{rel}) of optimised geometries for 4-*t*-butylphenyl-4-hydroxyazobenzene, **3**H.

Species	r_{NN}/Å	r_{CN}[a]/Å	∠NNC[b]/°	∠CNNC/°	Energy/ Hartree	ZPE/ Hartree	E_{rel}/ kJ mol^{-1}
E-**3**H	1.22	1.42	115.7	180.0	-800.126598	0.329236	0.0
		1.42	115.9				
Z-**3**H	1.22	1.43	124.5	5.6	-800.097733	0.328967	75.1
		1.43	124.2				
transition	1.20	1.44	117.6	72.3	-800.046548	0.326753	203.7
state		1.34	179.6				
S_1 state	1.24	1.39	126.5	113.2	-800.041250	0.326823	217.8
		1.39	126.5				

[a]The first and second r_{CN} refer to the 4-*t*-butylphenyl carbon and the 4'-hydroxybenzene carbon, respectively.
[b]The first and second ∠NNC refer to the 4-*t*-butylphenyl carbon and the 4'-hydroxybenzene carbon, respectively.

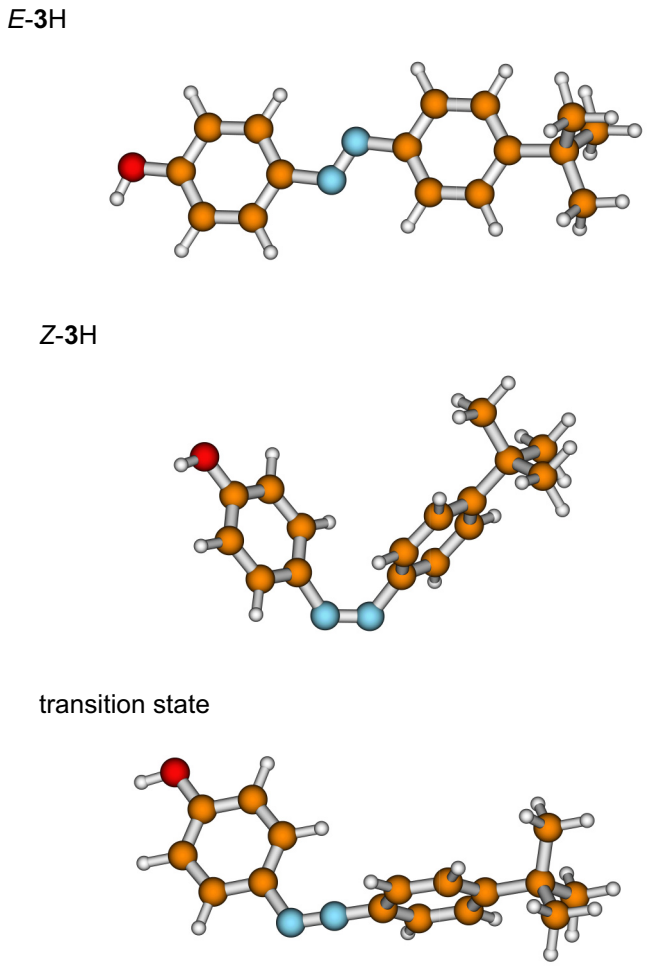

Fig. S11. Optimised geometries of stationary points on the ground electronic potential energy surface (S_0) of **3**H.

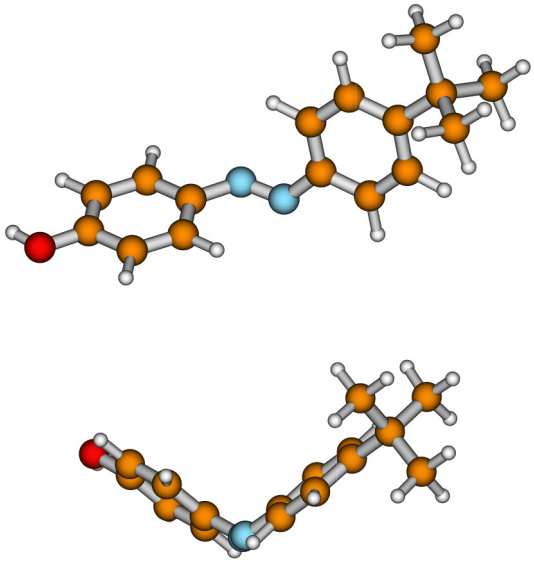

Fig. S12. Two views of the optimised geometry of the minimum energy conformation on the first excited state electronic potential energy surface (S_1) of **3**H. The lower view is along the N-N bond axis and shows the twisted geometry and transoid configuration.